

Phase transition systematics in BiVO₄ by means of high-pressure–high-temperature Raman experiments

J. Pellicer-Porres,^{1,*} D. Vázquez-Socorro,¹ S. López-Moreno,² A. Muñoz,³ P. Rodríguez-Hernández,³ D. Martínez-García,¹ S. N. Achary,⁴ A. J. E. Rettie,⁵ and C. Buddie Mullins⁵

¹MALTA Consolider Team, ICMUV, Universidad de Valencia, c/Dr. Moliner 50, 46100 Burjassot, Valencia, Spain

²CONACYT - División de Materiales Avanzados, IPICYT, Camino a la presa San José 20155, San Luis Potosí, S. L. P. 78216, Mexico

³Departamento de Física, Instituto de Materiales y Nanotecnología, MALTA Consolider Team, Universidad de La Laguna, E-38205 La Laguna, Tenerife, Spain

⁴Chemistry Division, Bhabha Atomic Research Centre, Trombay, Mumbai 400085, India

⁵McKetta Department of Chemical Engineering, The University of Texas at Austin, Austin, Texas 78712, US



(Received 3 September 2018; published 17 December 2018)

We report here high-pressure–high-temperature Raman experiments performed on BiVO₄. We characterized the fergusonite and scheelite phases (powder and single crystal samples) and the zircon polymorph (nanopowder). The experimental results are supported by *ab initio* calculations, which, in addition, provide the vibrational patterns. The temperature and pressure behavior of the fergusonite lattice modes reflects the distortions associated with the ferroelastic instability. The linear coefficients of the zircon phase are in sharp contrast to the behavior observed in the fergusonite phase. The boundary of the fergusonite-to-scheelite second-order phase transition is given by $T_{F-Sch}(K) = -166(8)P(\text{GPa}) + 528(5)$. The zircon-to-scheelite, irreversible, first-order phase transition takes place at $T_{Z-Sch}(K) = -107(8)P(\text{GPa}) + 690(10)$. We found evidence of additional structural changes around 15.7 GPa, which in the downstroke were found to be not reversible. We analyzed the anharmonic contribution to the wave-number shift in fergusonite using an order parameter. The introduction of a critical temperature depending both on temperature and pressure allows for a description of the results of all the experiments in a unified way.

DOI: [10.1103/PhysRevB.98.214109](https://doi.org/10.1103/PhysRevB.98.214109)

I. INTRODUCTION

Orthovanadate materials, with a composition given by AVO₄, where A is a trivalent metal or rare-earth ion, have a large number of technological applications [1–7]. BiVO₄, in particular, stirs special interest as a photocatalyst [8–10]. The photocatalytic activity of BiVO₄ strongly depends on the crystalline phase and morphology [10], with nanoparticles being of particular interest.

AVO₄ compounds mostly crystallize [11,12] in the zircon structure (Z, S. G. 141, *I4₁/amd*). Under high pressure, orthovanadates with light rare-earth cations (larger radii) transform to a monazite-type polymorph (M, S. G. 14, *P2₁/n*) [13–17]. However, zircon-type compounds with a small rare-earth cation present an irreversible transition to the scheelite phase (S, S. G. 88, *I4₁/a*) and a second transition to the fergusonite (F, S. G. 15, *I2/b*) at higher pressures [15,18–20].

In BiVO₄ the general scheme followed by orthovanadates is altered. BiVO₄ can be prepared with the zircon structure [21,22], but this phase is only metastable. Given the small radius of Bi compared to rare-earth elements, the scheelite phase could be expected to be the stable phase. However, the thermodynamically stable polymorph of BiVO₄ at ambient conditions is fergusonite [23]. It appears that the monoclinic symmetry of the fergusonite phase is the result of a distortion

of the tetragonal symmetry of the scheelite phase [23,24] by a ferroelastic instability [25]. Opposite to other orthovanadates, a second-order phase transition from the fergusonite to the scheelite phase is observed either at high pressure [26–28] [1.4(1) GPa] or high temperature [23,28–35] [525(3) K]. Another approach to stabilize the tetragonal scheelite phase is appropriate doping of the sample [36–38]. Additionally, the compound is found in nature with an orthorhombic structure called pucherite (S. G. 60, *Pnca*) [39].

Previous [26,30] Raman scattering experiments in the scheelite/fergusonite phases were focused on the lowest optical modes at the center of the Brillouin zone, which on the tetragonal paraelastic phase has *B_g* symmetry. The coupling of this mode with the ferroelastic distortion was suggested as the driving mechanism for the transition. Subsequent Brillouin experiments [31,32] demonstrated the existence of a soft acoustic mode and supported the proper character of the ferroelastic phase transition. The analysis of the angular dependence of the sound waves revealed [31] perfect softening of the transversal acoustic branch along a direction in the tetragonal (001) plane. Inelastic neutron scattering [33] characterized the softening of the transversal acoustic branch along [0.7ξ, ξ, 0]. The dispersion curve showed an upward curvature which could not be completely determined, thus limiting the conclusions extracted about the associated elastic constant, which did not manifest complete softening.

In this work we complement previous Raman experiments describing the behavior of the whole set of Raman active

*Julio.Pellicer@uv.es

modes as well as extending the pressure range and introducing simultaneously high-pressure–high-temperature conditions. The scheelite phase is destabilized at 15.7 GPa. The high-pressure behavior of zircon will be discussed. The experimental findings are supported by *ab initio* calculations, which in addition provide the vibrational pattern. Finally, we use the Landau theory to discuss the full set of high-pressure–high-temperature experiments. The paper is organized as follows. In Sec. IV A the ambient conditions results are described, including the characterization of the modes in terms of symmetry, vibration patterns, and relationships between the three phases. Section IV B is devoted to high-pressure and high-temperature results, beginning with a description of pressure and temperature coefficients, then describing the phase boundaries, and finally analyzing how the anharmonic interactions affect the wave-number shifts in the fergusonite structure.

II. EXPERIMENT

The BiVO₄ samples used in the Raman experiments had different origins. Single crystals adopting the fergusonite structure were grown by the floating zone technique [40,41]. Zircon BiVO₄ is prepared by a precipitation method from the acidic aqueous solution of Bi(NO₃)₃ and NH₄VO₃ at room temperature [42]. Polycrystalline fergusonite in powder form was purchased from Alfa-Aesar (CAS 14059-33-7, 99.9% purity).

High-pressure Raman measurements were performed using a diamond anvil cell having a 16:3:1 methanol-ethanol-water mixture or Ne as a pressure-transmitting medium [43]. The sample was loaded into a cylindrical pressure chamber with a diameter of 100–200 μm and a thickness between 40 and 50 μm, which was holed in the center of the stainless steel gasket. Pressure was determined using ruby luminescence [44]. Raman spectra were collected in the backscattering geometry using a 632.8-nm He-Ne laser and a Jobin-Yvon spectrometer in combination with a thermoelectric-cooled multichannel CCD detector with spectral resolution around 2 cm⁻¹. A laser power of less than 2 mW before the diamond anvil cell was necessary to avoid the fergusonite-to-scheelite phase transition induced by sample heating. High-temperature experiments at ambient pressure were conducted in an air atmosphere. Temperature was measured via Pt resistance. High-pressure–high-temperature experiments were carried out employing external heating. Temperature was established by the calibrated reading of a thermocouple in close contact with the diamonds. In this setup, pressure was determined using the fluorescence line of SrB₄O₇ : Sm²⁺ [45].

III. CALCULATIONS

Calculations of the total energy were performed within the framework of the density functional theory (DFT) [46] and the projector-augmented wave (PAW) [47,48] method as implemented in the Vienna *Ab initio* Simulation Package (VASP) [49–52]. A plane-wave energy cutoff of 600 eV was used to ensure a high precision in our calculations. The exchange-correlation energy was described with the HSE06 hybrid functional [53–56]. This functional has been used with success

in the study of other vanadates such as InVO₄ and FeVO₄ [57,58]. The Monkhorst-Pack scheme [59] was employed to discretize the Brillouin zone (BZ) integrations with meshes 3 × 3 × 3, 4 × 4 × 2, and 3 × 2 × 4, which correspond to a set of 6, 4, and 6, special *k*-points in the irreducible BZ for the zircon, scheelite, and fergusonite phases, respectively. In the relaxed equilibrium configuration, the forces are less than 2 meV/Å per atom in each of the Cartesian directions. This high degree of convergence is required for the calculations of vibrational properties using the direct force constant approach [60]. High-pressure lattice dynamic calculations were carried out at the zone center (Γ point) of the BZ.

IV. RESULTS AND DISCUSSION

A. Raman in ambient conditions

1. Mode characterization

We begin our description with the fergusonite phase. A group symmetry analysis yields 18 Raman active modes

$$\Gamma_R(F) = 8A_g + 10B_g, \quad (1)$$

where the A_g (B_g) modes are symmetrical (antisymmetrical) with respect to the twofold *c*-axis. The Raman tensors of the modes are

$$R_{A_g} = \begin{pmatrix} a & d & 0 \\ d & b & 0 \\ 0 & 0 & c \end{pmatrix}, \quad R_{B_g} = \begin{pmatrix} 0 & 0 & e \\ 0 & 0 & f \\ e & f & 0 \end{pmatrix}. \quad (2)$$

Our single crystals have their largest surface oriented perpendicular to the *c*-axis. When using single crystals we have only access to A_g modes. In the experiments with the sample in powder form all the modes are allowed. A key to the identification of B_g modes has been its observation in powder spectra but not in single crystals (Fig. 1). Table I presents a summary of the results. We include the wave numbers and symmetries yielded by the *ab initio* calculations performed with the hybrid functional HSE06, as well as the results corresponding to the single crystal study reported in Ref. [34]. The B_g^1 , B_g^2 , and A_g^1 modes are too low in energy to be accessible in our Raman setup (edge filter cutoff around 70 cm⁻¹). The B_g^5 mode at 241(1) cm⁻¹ is very weak. It was not reported in Ref. [34]. Its identification is supported by *ab initio* computations. The agreement between experiment and theory is in general satisfactory, though it is worse for the highest energetic modes. From the experimental point of view the identification of the B_g^9 , A_g^7 , and A_g^8 modes is straightforward. Although the presence of the B_g^{10} mode is clear, its precise wave-number characterization is troublesome due to the nearby presence of strong modes.

The Raman active modes in the scheelite phase are given by

$$\Gamma_R(S) = 3A_g + 5B_g + 5E_g. \quad (3)$$

The scheelite phase is not stable in ambient conditions. The spectra obtained at either high pressure or high temperature are presented in Fig. 2. To compare the wave numbers measured with those of the fergusonite and zircon phases it is possible to extrapolate either the high-pressure or the high-temperature values to ambient conditions. The results

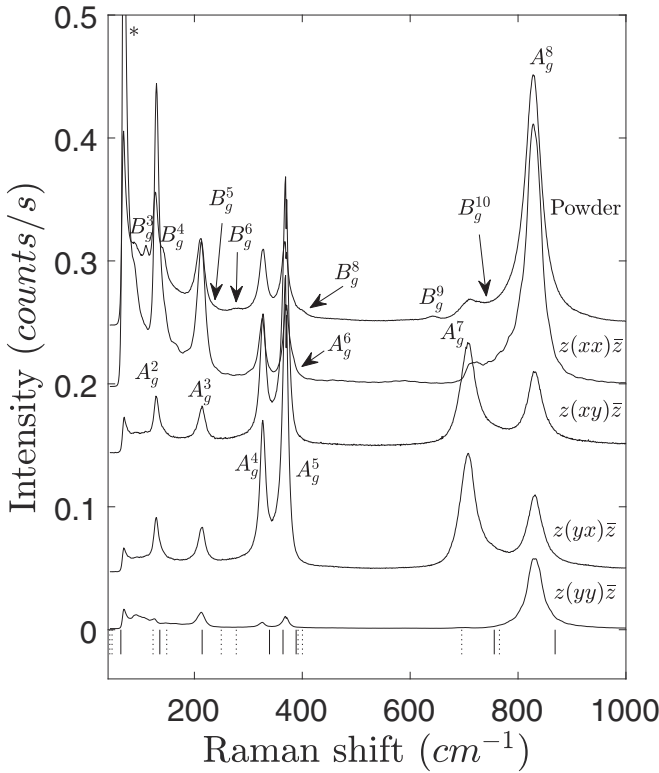


FIG. 1. Symmetry assignment of Raman modes in the fergusonite phase by comparison of single crystal polarized spectra with the spectrum of the sample in powder form. In single crystal spectra B_g modes are not allowed. The spectra have been shifted for clarity. Continuous (dashed) lines at the bottom correspond to the *ab initio* calculation for the A_g (B_g) modes. The peak labeled with a star is a glitch originated by the edge filter.

are compiled in Table II. We observe that both extrapolations agree. High-pressure experiments do not involve widening of the modes, as it does happen in high-temperature conditions. It is then possible to identify the weakest modes: B_g^2 , E_g^3 , B_g^4 , and E_g^5 . Symmetry assignments are based on comparison with *ab initio* calculations, pressure coefficients, and correlation between the fergusonite and scheelite phases (see below).

Finally, the Raman active modes in the zircon phase belong to the following representations:

$$\Gamma_R(Z) = 2A_{1g} + 4B_{1g} + B_{2g} + 5E_g, \quad (4)$$

where the A_{1g} and B_{2g} modes only involve oxygen movements. We present in Fig. 3 the ambient pressure Raman spectrum corresponding to ambient conditions. We identified 10 out of the 12 modes, as indicated in Table III. Compared to previous results [61] we provided additional information on the weak modes at 194 cm⁻¹ (E_g^3) and 429 cm⁻¹ (B_g^3). The symmetry assignment has been performed with the aid of *ab initio* calculations. The agreement between the computed and measured values is within 6% for most of the modes. In Fig. 3 there is an additional mode marked with a star whose position is close to the most intense peak of the fergusonite phase. We suggest that it is associated to a residual compo-

TABLE I. Raman frequencies, pressure coefficients, and temperature coefficients corresponding to the active Raman modes in the fergusonite structure in ambient conditions. ω is expressed in cm⁻¹, P in GPa and T in K.

Mode	Experiment			Ref. [34]	Calculations	
	ω_0	$\partial\omega/\partial P$	$10^3 \cdot \partial\omega/\partial T$	ω_0	ω_0	$\partial\omega/\partial P$
B_g^1				47	43(2)	4.7(2)
B_g^2				55	47(2)	6.1(3)
A_g^1				62	64(3)	-1.2(1)
B_g^3	111(2)	1.2(4)	38(7)	110	123(6)	0.9(1)
A_g^2	129(1)	-4.6(2)	-38(2)	130	136(7)	-2.9(1)
B_g^4	141(1)	-2.1(2)	-42(4)	144	149(7)	-2.3(1)
A_g^3	213(1)	2.0(1)	-32(4)	212	214(11)	0.5(1)
B_g^5	241(1)				250(13)	6.9(3)
B_g^6	276(1)	-2.1(3)	-80(30)	280	278(14)	-1.4(1)
A_g^4	327(1)	3.8(3)	30(30)	326	339(17)	4.8(2)
A_g^5	369(1)	-3.6(2)	-36(8)	370	364(18)	-2.8(1)
A_g^6	383(1)	2.1(2)		386	389(19)	0.9(1)
B_g^7					392(20)	1.3(1)
B_g^8	400(1)			400	400(20)	-0.6(1)
B_g^9	641(1)	7.6(2)	19(4)	642	700(40)	13.0(7)
A_g^7	708(1)	0.2(3)	-9(7)	711	760(40)	5.0(3)
B_g^{10}	747(5)			743	770(40)	-9.0(5)
A_g^8	831(1)	-8.1(3)	-64(2)	830	870(40)	-2.6(1)

nent of the fergusonite phase. As the zircon phase is pure from the point of view of x-ray diffraction, the proportion of the fergusonite phase should be very small (less than 5% approximately).

2. Vibration patterns

Scheelite, fergusonite, and zircon structures share structural characteristics [11]. The most relevant is the existence of tetrahedral VO₄ units with strong covalent bonds. The O atoms around the Bi atoms define BiO₈ bisdisphenoids which can be visualized as formed by two interpenetrating tetrahedra, one compressed and one elongated. The bisdisphenoids are connected by edges, forming zig-zag chains. The connectivity between the chains and VO₄ tetrahedra differs in scheelite and zircon. Both structures have tetragonal symmetry. However, the packing is not as efficient in the zircon structure as it is scheelite, resulting in a unit cell volume slightly larger in zircon than in scheelite. Fergusonite results from the scheelite following a monoclinic distortion associated to the ferroelastic instability. The fergusonite-to-scheelite transformation is related to a second-order phase transition [23–25]. The reduction in symmetry in fergusonite with respect to scheelite is related to the loss of the fourfold screw axis which implies the following correlations: $A_g, B_g(S) \rightarrow A_g(F)$, $E_g(S) \rightarrow 2B_g(F)$. These correlations are best represented in Fig. 4 by the splitting of the E_g^2 mode into B_g^3 and B_g^4 as well as by the transformation of B_g^5 into A_g^7 or A_g^1 into A_g^3 . On the opposite, the transformation from zircon to scheelite is a first-order phase transition implying substantial bond reorganization. Consequently, the modes involved in analogous

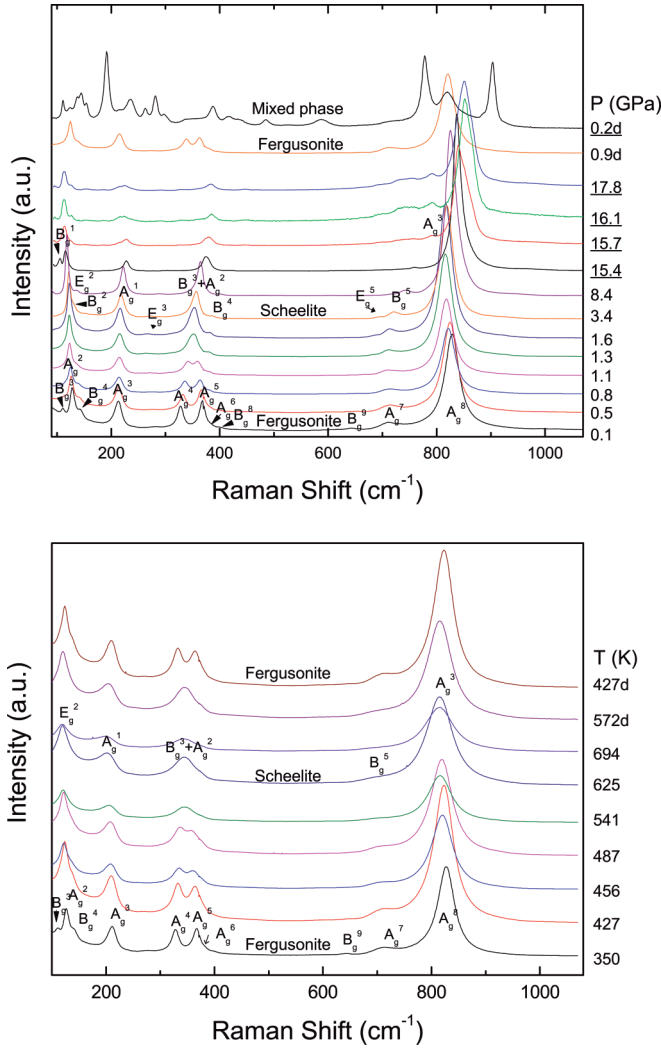


FIG. 2. Raman spectra corresponding to the fergusonite polymorph. Upper panel: Selected high-pressure spectra. Numbers next to the spectra indicate pressure in GPa, either in the upstroke or downstroke. Spectra correspond to the different experiments, either with a 16:3:1 methanol:ethanol:water as pressure transmitting medium or Ne (underlined pressures) Lower panel: Selected spectra at different temperatures (K).

correlations [$A_{1g}, A_{2g}(Z) \rightarrow A_g(S), B_{1g}, B_{2g}(Z) \rightarrow B_g(S), E_g(Z) \rightarrow E_g(S)$] are affected by discontinuous changes in wave number and their relationship is not so clear. In Fig. 5 it would seem that $A_{1g}^2 \rightarrow A_g^3, B_{1g}^4 \rightarrow B_g^5, B_{1g}^3 \rightarrow B_g^3, A_{1g}^1 \rightarrow A_g^2, B_{2g}^1 \rightarrow B_g^2, E_g^2 \rightarrow E_g^2$. The A_g^1 would originate from the silent A_{2g}^1 mode which the calculations situate at 176 cm^{-1} .

As stated above, the three structures share the presence of VO_4 tetrahedra. This fact suggests a discussion of lattice vibrations in terms of modes of the tetrahedra. The internal modes of the tetrahedra (A_1, E , and $2F_2$) are labeled ν_1, ν_2, ν_3 , and ν_4 . The rotational (F_1) and translational (F_2) are denoted R and T , respectively, whereas the contribution from Bi atoms are labeled Bi. Considering that there are two tetrahedra and two Bi atoms in each primitive unit cell, the Raman active modes in scheelite and zircon phases can be

TABLE II. Raman frequencies, pressure coefficients, and temperature coefficients corresponding to the active Raman modes in the scheelite structure. Wave numbers were extrapolated to ambient conditions from high pressure (HP) and high temperature (HT) experiments. ω is expressed in cm^{-1} , P in GPa and T in K.

Mode	Experiment				Calculations	
	ω_0 (HP)	ω_0 (HT)	$\partial\omega/\partial P$	$10^3 \cdot \partial\omega/\partial T$	ω_0	$\partial\omega/\partial P$
E_g^1					19(2)	8.7(4)
B_g^1	67(2)		2.4(2)		32(2)	5.6(3)
B_g^2	124(1)		1.4(1)		127(6)	0.9(1)
E_g^2	124(1)	124(1)	-0.5(1)	-11(1)	141(7)	-0.3(1)
A_g^1	214(1)	211(1)	0.9(1)	-26(1)	219(11)	0.9(1)
E_g^3	265(1)		2.7(1)		256(13)	3.5(2)
A_g^2	349(1)	348(1)	1.7(1)	-9(2)	346(17)	0.9(1)
B_g^3					346(18)	2.7(1)
B_g^4	377(1)		2.8(1)		385(19)	2.0(1)
E_g^4					390(20)	1.3(1)
E_g^5	676(2)		4.7(2)		720(40)	4.1(2)
B_g^5	711(1)	716(4)	3.2(1)	-48(13)	750(40)	3.3(2)
A_g^3	813(1)	817(1)	1.6(1)	-8(1)	850(40)	4.0(2)

classified as

$$\begin{aligned} \Gamma_R(S) &= \nu_1(A_g) + \nu_2(A_g) + \nu_2(B_g) + \nu_3(B_g) + \nu_3(E_g) \\ &\quad + \nu_4(B_g) + \nu_4(E_g) + T(B_g) + T(E_g) + R(A_g) \\ &\quad + R(E_g) + \text{Bi}(B_g) + \text{Bi}(E_g), \\ \Gamma_R(F) &= \nu_1(A_g) + 2\nu_2(A_g) + \nu_3(A_g) + 2\nu_3(B_g) + \nu_4(A_g) \\ &\quad + 2\nu_4(B_g) + T(A_g) + 2T(B_g) + R(A_g) \\ &\quad + 2R(B_g) + \text{Bi}(A_g) + 2\text{Bi}(B_g), \\ \Gamma_R(Z) &= \nu_1(A_{1g}) + \nu_2(A_{1g}) + \nu_2(B_{2g}) + \nu_3(B_{1g}) + \nu_3(E_g) \\ &\quad + \nu_4(B_{1g}) + \nu_4(E_g) + T(B_{1g}) + T(E_g) \\ &\quad + R(A_{2g}) + R(E_g) + \text{Bi}(B_{1g}) + \text{Bi}(E_g). \end{aligned} \quad (5)$$

TABLE III. Raman frequencies, pressure coefficients, and temperature coefficients corresponding to the active Raman modes in the zircon structure in ambient conditions. ω is expressed in cm^{-1} , P in GPa, and T in K.

Mode	Experiment			Ref. [61]	Calculations	
	ω_0	$\partial\omega/\partial P$	$10^3 \cdot \partial\omega/\partial T$		ω_0	$\partial\omega/\partial P$
B_{1g}^1					60(3)	3.0(2)
E_g^1					67(3)	3.2(2)
E_g^2	112(2)	5.2(7)	10(2)	113	133(7)	-0.7(1)
B_{1g}^2	179(2)		-30(8)	186	193(10)	2.1(1)
E_g^3	194(1)	3.6(3)	-32(8)		203(10)	3.8(2)
B_{1g}^1	248(1)	-1.1(1)	3(1)	248	269(13)	-1.9(1)
E_g^4	346(3)	0.9(5)	34(6)	348	359(18)	0.6(1)
A_{1g}^1	367(1)	1.2(2)	9(1)	367	366(18)	1.5(1)
B_{1g}^3	429(1)	1.3(7)	-6(7)		440(20)	1.8(1)
E_g^5	734(5)	5.7(6)	80(30)	732	780(40)	4.7(2)
B_{1g}^4	763(6)	8.1(8)	-31(6)	761	810(40)	6.2(3)
A_{1g}^2	857(1)	5.2(3)	-12(1)	856	900(50)	5.4(3)

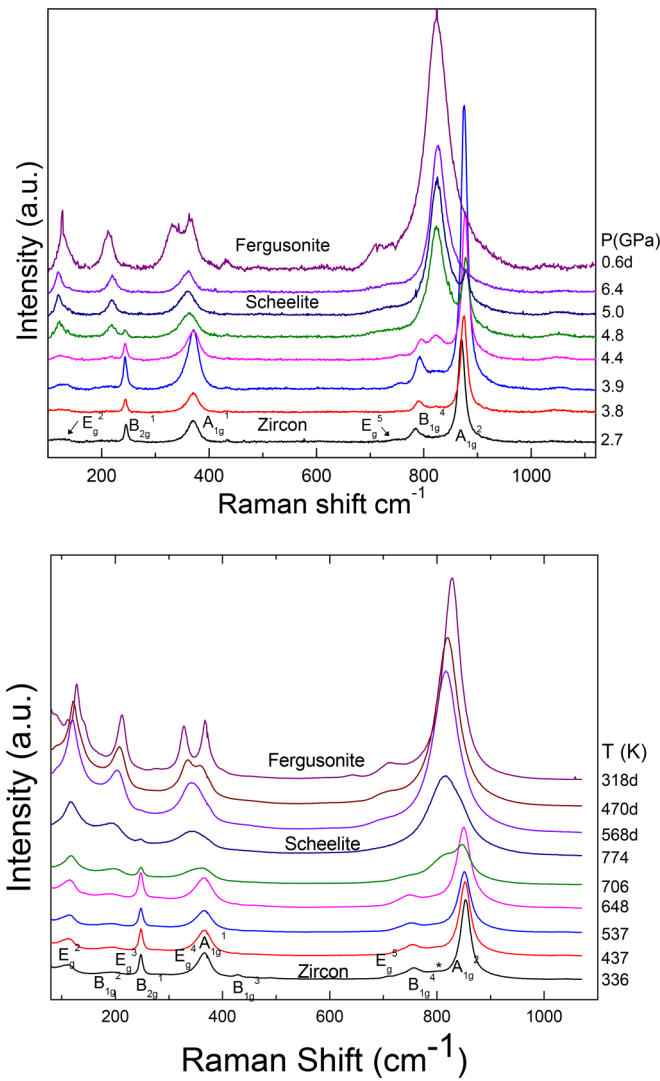


FIG. 3. Raman spectra corresponding to the zircon polymorph. Upper panel: Selected high-pressure spectra. Numbers next to the spectra indicate pressure in GPa, (d) either in the upstroke or downstroke. Methanol-ethanol-water is used as pressure transmitting medium. Lower panel: Selected spectra at different temperatures (K).

The tetrahedra ν_1 mode is only strictly stretching in the zircon and scheelite phases. The A_{1g}^2 mode in zircon (Fig. 6) is the one with the highest frequency (857 cm^{-1}). This is due to the contribution of Bi–O bonds, which in the scheelite A_g^3 (813 cm^{-1}) mode are bent and in zircon are also slightly stretched. In the fergusonite A_g^8 mode (831 cm^{-1}) the Bi–O bonds are also stretched. The frequency decreases with respect to the zircon phase because now the movement of oxygen atoms is not exactly directed along V–O bonds. In zircon and scheelite, only oxygen atoms can vibrate. In fergusonite, V and Bi atoms are allowed to move by symmetry, but the calculation shows that the amplitude of movement is one order of magnitude smaller than that of O atoms.

In scheelite, the second-highest Raman allowed mode corresponds to B_g^5 (711 cm^{-1}), which is a ν_3 asymmetric stretching bond where V is nearly at rest. Bi–O bonds continue bending. The corresponding mode in fergusonite is the A_g^7

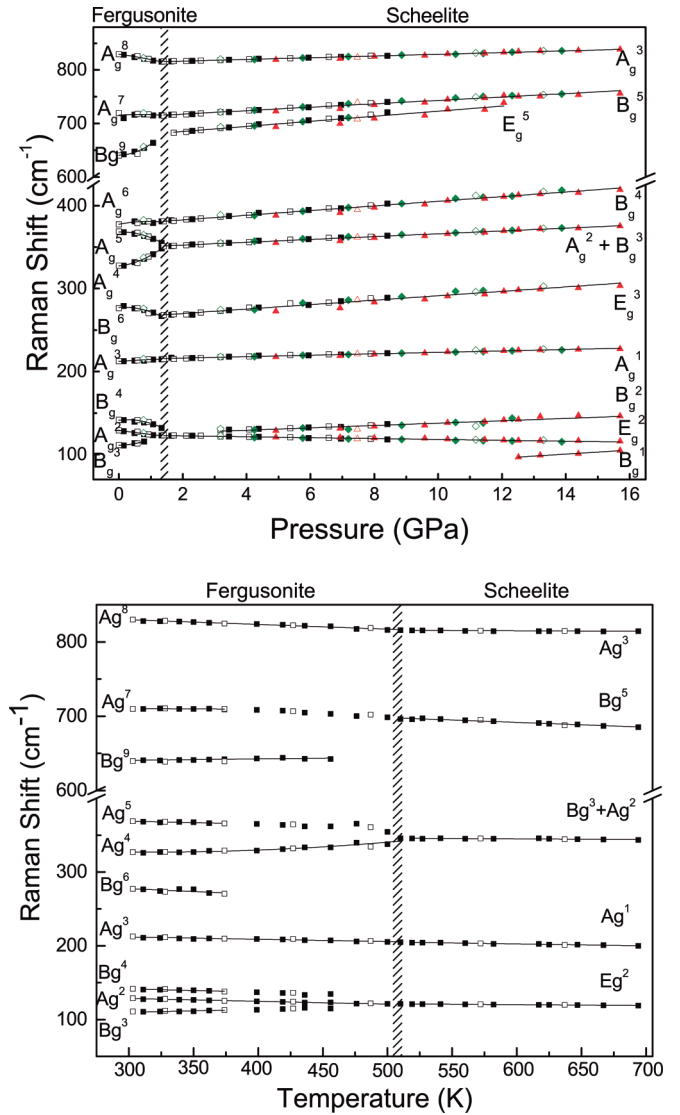


FIG. 4. Upper panel: Pressure dependence of the Raman modes of fergusonite BiVO₄. The three different symbols represent three separate experiments. Squares correspond to an experiment in which the sample is in powder form and a 16:3:1 methanol-ethanol-water mixture is used as pressure transmitting medium. Diamonds experiment was carried out with a single crystal and Ne as pressure transmitting medium. Triangles represent an experiment where fergusonite powder and Ne were used. Filled (hollow) symbols were obtained in the upstroke (downstroke). Lower panel: Temperature dependence of the Raman modes of fergusonite structure.

mode (708 cm^{-1}). The vibration pattern is similar to that of scheelite but with the stretching slightly misaligned with respect to the V–O bond. In zircon, the B_{1g}^4 mode (763 cm^{-1}) displays a higher frequency due to the contribution of V atoms to the stretching. The remaining ν_3 mode corresponds to the E_g^5 mode in both scheelite (676 cm^{-1}) and zircon (734 cm^{-1}), Fig. 6. In fergusonite it is related to a couple of modes, B_g^9 (641 cm^{-1}) and B_g^{10} (747 cm^{-1}). In each of these modes a different pair of O atoms vibrate against the V atom.

The modes appearing in the spectral range between 130 and 450 cm^{-1} are not so readily classifiable in terms of the

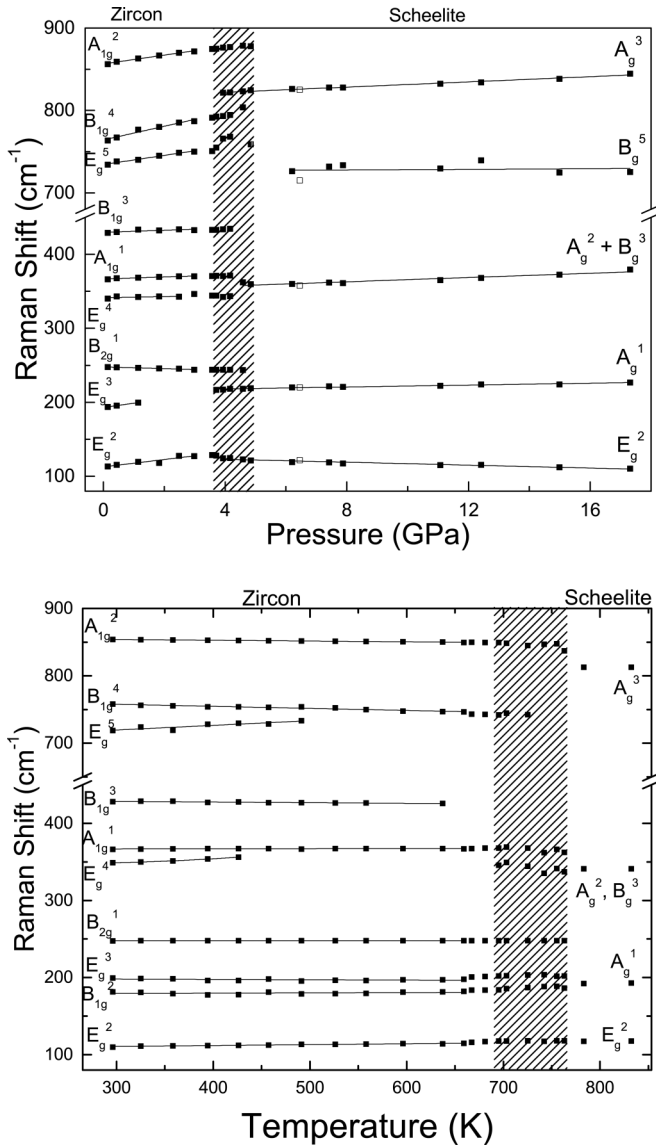


FIG. 5. Raman modes of the zircon polymorph. Upper panel: Pressure dependence. Lower panel: Temperature dependence.

tetrahedral vibration. The phonon patterns reveal characteristics which can be described as a blend of bending [ν_2 , scissor (ν_4)], translational (T), or rotational modes (R). In the most symmetric zircon structure some of the modes can be identified (Fig. 6): A_{1g}^1 (R , 176 cm^{-1} , silent mode), B_{1g}^2 (T , 179 cm^{-1}), E_g^4 (ν_4 , 346 cm^{-1}), and A_{1g}^1 (ν_2 , 367 cm^{-1}).

The least energetic modes are the only ones in which Bi atoms vibrate with nonnegligible amplitudes. In zircon, Bi atoms vibrate along the c -axis in B_{1g}^1 (60 cm^{-1}) or in the perpendicular direction, as in E_g^1 (67 cm^{-1}). Bi atoms connected by glide planes shift in opposite directions. V atoms are at rest. In scheelite, Bi atoms vibrate along the c axis in the B_g^1 mode. Bi atoms and V atoms with the same x and y atomic coordinate shift in the same direction. In the E_g^1 mode Bi atoms have a large amplitude in the direction perpendicular to the c -axis. The amplitude of V and O atoms is one order of magnitude smaller. In fergusonite, the B_g^1 and B_g^2 (43 and

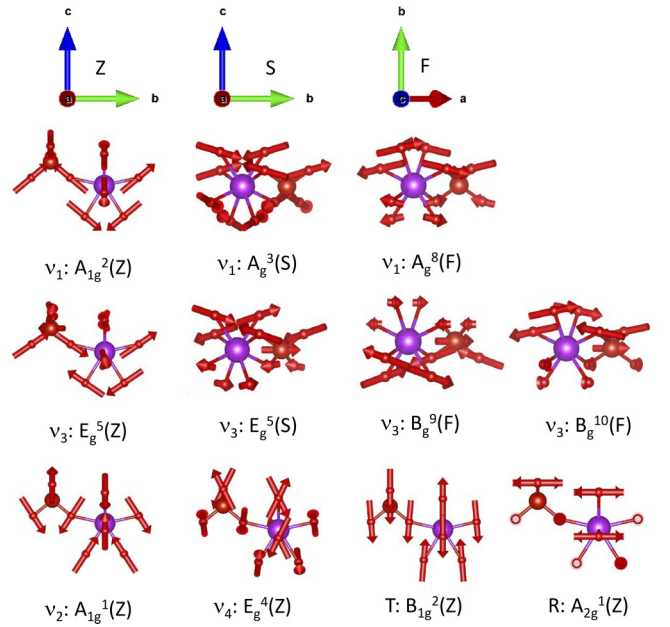


FIG. 6. Selected patterns of lattice vibrations at the gamma point in zircon (Z), scheelite (S) and fergusonite (F). Large, medium and small spheres represent Bi, V, and O atoms, respectively. We represent only the first neighbor cell of V and Bi atoms. Modes labeled ν , T , and R are derived from the internal, translational, and rotational modes of the VO_4 tetrahedra.

47 cm^{-1}) modes display Bi movement perpendicular to the binary axis, whereas in the A_g^1 (62 cm^{-1}) mode the movement is along the binary axis. V atoms only move in B_g^1 .

B. High-pressure and high-temperature studies

1. Pressure and temperature coefficients

We focus first on pressure and temperature coefficients. The wave-number dependence is linear in scheelite, slightly differs from linearity in zircon and is more complex in the fergusonite structure. The coefficients presented in Tables I and III were obtained using data obtained near ambient conditions, where the dependence either in pressure or temperature is linear. The data of the pressure coefficients largely coincide with those obtained with *ab initio* calculations, in both value and the sign. Only the pressure coefficients associated with the E_g^2 mode of the zircon phase and the B_g^9 , A_g^7 , and A_g^8 modes of the fergusonite phase differ significantly from the coefficients obtained from the simulation. In Ref. [24], high-pressure and high-temperature x-ray diffraction studies were compared plotting the lattice parameters as a function of volume, concluding that lattice axes depend linearly on relative volume, independent of temperature or pressure. If this is the case, and harmonic effects prevail, signs in pressure and temperature coefficients should be opposite. This is, in fact, what is observed in the scheelite structure. In the zircon polymorph nearly half of the modes follow this rule, whereas in fergusonite nearly all of them show pressure and temperature coefficients with the same sign. We conclude that anharmonic effects determine decisively the lattice dynamics in the fergusonite structure, they are also present in the zircon

structure but they are not evident in the scheelite structure. Anharmonic effects will be further discussed in Sec. IV E.

2. Phase transitions

Figure 2 presents the evolution of Raman spectra of fergusonite BiVO₄ under high pressure (upper panel) or temperature (lower panel). Merging of A_g^4 and A_g^5 modes on the one hand and B_g^3 , A_g^2 , and B_g^4 on the other, is readily appreciable when pressure or temperature increases, up to the fergusonite-to-scheelite phase transition. When extreme conditions are relaxed, the sample reverts to the fergusonite structure. The wave numbers measured in the downstroke or on cooling do not show any hysteresis (void symbols in Fig. 4), in agreement with the reversible character of the phase transition [24,27,29]. From combined high-pressure–high-temperature experiments (not shown), we determine the boundary of the fergusonite-to-scheelite phase transition as given by

$$T_{F-Sch} = -166(8) * P + 528(5), \quad (6)$$

where temperature is in GPa and T in K. As a comparison, the boundary is given by $T_{F-Sch} = -150(8) * P + 523(3)$ following Ref. [27] or $dT_{F-Sch}/dP = -166(8)$ in Ref. [26].

Figure 3 shows the behavior of Raman spectra of zircon BiVO₄ from 0 to 6.4 GPa (upper panel) and from room temperature to 774 K (lower panel). In both cases the emergence of the A_g^3 (213 cm⁻¹) and A_g^8 (831 cm⁻¹) modes indicates the transition to the scheelite structure. The phase transition is gradual. The range of pressure/temperature values where both phases coexist has been greyed in Fig. 5. Using as a criteria the destabilization of the zircon structure, as indicated by the appearance of the first fergusonite peaks in combined high-pressure–high-temperature experiments (not shown), the phase transition boundary is determined to be

$$T_{Z-Sch} = -107(8) * P + 690(10). \quad (7)$$

The transition from the zircon to the scheelite phase was determined [22] to range between 673 to 773 K by combined differential thermal analysis (DTA) and XRD of quenched samples. Subsequent [42] DTA studies yielded temperatures between 623 and 723 K. Up to our knowledge, there are not previous studies on the high-pressure stability of zircon BiVO₄. However, there has been a lot of work on the high-pressure behavior of other zircon orthovanadates. The transition pressure from the zircon to the scheelite [62] structure is always a few gigapascals.

The range of stability of the scheelite phase is small. In Fig. 2 we show spectra corresponding to higher pressures. At 15.7 GPa new modes appear. The A_g^1 mode is doubled. The sample becomes very inhomogeneous, as qualitatively different spectra are measured in different parts of the sample. From Raman studies alone we cannot discard sample decomposition. This behavior has been observed irrespective of the pressure transmitting medium employed (MEW or Ne), sample form (powder or single crystal), or initial crystalline structure (fergusonite or zircon). The destabilization of the scheelite phase is observed at lower pressures (13.8 GPa) if less hydrostatic pressure transmitting media are used (MEW). The changes observed are irreversible since the spectrum

recovered from 17.8 GPa is different from the initial fergusonite phase.

3. Order parameter

We pointed out in Sec. IV C the strong anharmonic behavior of lattice modes of the fergusonite structure as revealed by the sign of pressure and temperature coefficients. We are going now to deepen the relationship between the anharmonic behavior of the modes and the static distortion which stabilizes the monoclinic distortion. According to lattice dynamical theory [63] the anharmonic coupling (quantified by α_k) of any phonon (wave number ω_k) with the order parameter (η) results in a modification of the phonon wave number given by $\tilde{\omega}_k^2 = \omega_k^2 + 1/2\alpha_k\eta^2$.

We also saw in Sec. IV A 2 that the E_g^2 mode in scheelite gives raise to the B_g^3 and B_g^4 modes in fergusonite. In the absence of the static distortion both modes would have the same wave number. We can write then

$$\eta = \frac{2(\omega_{B_g^4}^2 - \omega_{B_g^3}^2)}{\alpha_{B_g^4} - \alpha_{B_g^3}}. \quad (8)$$

The pressure and temperature behavior of the A_g^5 and A_g^6 modes is also clearly correlated. However, in this case they do not originate from a doublet mode in scheelite, but from the B_g^3 and A_g^2 modes, which are accidentally degenerated. It seems reasonable to assume that without the anharmonic interaction they would continue to be degenerated. We can approximate

$$\eta \simeq \frac{2(\omega_{A_g^6}^2 - \omega_{A_g^5}^2)}{\alpha_{A_g^6} - \alpha_{A_g^5}}. \quad (9)$$

The free energy can be written [63] as a Landau expansion as

$$F(\eta) = F(0) + \frac{1}{2}A(T - T_c)\eta^2 + \frac{1}{4}B\eta^4, \quad (10)$$

where A and B are constants and T_c is considered to depend on both pressure and temperature as given in Eq. (6). Minimizing the free energy leads to an alternate expression of the order parameter

$$\eta = \sqrt{\frac{A}{B}(T_c[T, P] - T)}. \quad (11)$$

Figure 7 tests the theory just described comparing either Eq. (8) or (9) with Eq. (11), in the whole set of high-pressure–high-temperature experiments performed. The linear fits displayed in Fig. 7 are described by: $\log[\Delta(A_g^5 - A_g^4)] = 0.50(2)(T_c(P) - T) + 3.31(4)$, $\log[\Delta(B_g^4 - B_g^3)] = 0.46(4)(T_c(P) - T) + 2.81(5)$. The critical exponent of the fergusonite-to-scheelite phase transition is then 1/2, as expected in a second-order phase transition.

V. CONCLUSION

We discussed 11 Raman experiments, (corresponding to three BiVO₄ polymorphs, fergusonite, scheelite, and zircon; under high pressure, high temperature, or a combination of both. Our results are interpreted with the aid of *ab initio* calculations.

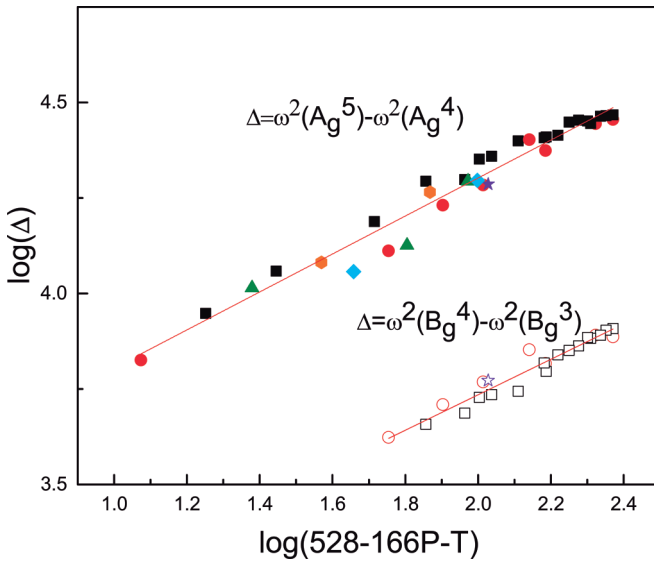


FIG. 7. Analysis of the order parameter as pressure and/or temperature is varied. Δ is proportional to the order parameter [Eqs. (8) and (9)]. Pressure and temperature are combined as in Eq. (6). Symbols correspond to different experiments. Squares: ambient pressure, temperature variation; circles and stars: ambient temperature, pressure variation; triangles: $T = 331$ K, pressure variation; rhombs: $T = 342$ K, pressure variation; hexagons: $T = 391$ K, pressure variation.

We determine the wave numbers of previously uncharacterized modes of the three phases. The modes of the three structures are related based not only on their symmetry but also on their relationship with the VO_4 tetrahedra. *Ab initio* calculations provide the phonon patterns, which were not available in the literature.

High-pressure and high-temperature studies reveal a qualitatively different behavior of the three phases. Pressure and temperature induce a linear shift of wave numbers in scheelite. In the zircon phase the shift is slightly nonlinear, whereas in the fergusonite phase it is more complex. We determine pressure and temperature coefficients for the three phases. The behavior of the fergusonite phase is decisively affected

by anharmonic effects, which are evidenced by the sign of their pressure and temperature coefficients. We analyzed the anharmonic contribution to the wave-number shift using an order parameter. The introduction of a critical temperature depending both on temperature and pressure allows the description of the results of all the experiments in a unified way.

Fergusonite transforms to the scheelite phase under high pressure or high temperature. The phase transition boundary is given by Eq. (6). It is a reversible second-order phase transition. We show that the critical exponent associated to the transition is $1/2$. Zircon also transforms to the scheelite phase under high pressure or temperature, but this time the transition is first order and irreversible. The zircon phase is destabilized at pressures and temperatures given by Eq. (7). The scheelite phase is stable up to 15.7 GPa. The modifications observed in the spectra are partially retained when high pressure is released.

ACKNOWLEDGMENTS

This work has been supported by Ministerio de Economía, Industria y Competitividad under The National Program of Materials (Grant Nos. MAT2013-46649-C4-1-P, MAT2016-75586-C4-1-P/3-P) and The Consolider-Ingenio 2010 Program (MALTA CSD2007-0045) and by the EU-FEDER funds. D. Vázquez wishes to thank Ministerio de Industria, Ciencia y Competitividad for the FPI grant (BES-2014-068953). A.J.E.R. and C.B.M. thank the Welch Foundation (F-1436) and the US Department of Energy Basic Energy Sciences (Grant no. DE-FG02-09ER16119) for their generous support. S.L.-M. thanks CONACYT of México for financial support through the program “Catedras para Jóvenes Investigadores.” P.R.-H. acknowledge computing time provided by Red Española de Supercomputación (RES) and MALTA-Cluster. The authors gratefully acknowledge the computing time granted by LANCAD and CONACYT on the supercomputer Miztli at LSVP DGTIC UNAM. Also, some of the computing for this project was performed with the resources of the IPICYT Supercomputing National Center for Education & Research, grant TKII-R2018-SLM1.

- [1] W. Ryba-Romanowski, *Cryst. Res. Technol.* **38**, 225 (2003).
- [2] S. Miyazawa, *Opto-Electronics Review* **11**, 77 (2003).
- [3] M. Oshikiri, M. Boero, A. Matsushita, and J. Ye, *J. Chem. Phys.* **131**, 034701 (2009).
- [4] K. Fukudome, N.-O. Ikenaga, T. Miyake, and T. Suzuki, *Catal. Sci. Technol.* **1**, 987 (2011).
- [5] C.-J. Jia, L.-D. Sun, F. Luo, X.-C. Jiang, L.-H. Wei, and C.-H. Yan, *Appl. Phys. Lett.* **84**, 5305 (2004).
- [6] A. A. Kaminskii, H. Rhee, H. J. Eichler, K. Ueda, K. Oka, and H. Shibata, *Appl. Phys. B* **93**, 865 (2008).
- [7] A. A. Kaminskii, O. Lux, H. Rhee, H. J. Eichler, K. Ueda, H. Yoneda, A. Shirakawa, B. Zhao, J. Chen, J. Dong, and J. Zhang, *Laser Phys. Lett.* **9**, 879 (2012).
- [8] C. M. Suarez, S. Hernández, and N. Russo, *Appl. Catal. A: General* **504**, 158 (2015).
- [9] Q. Jia, K. Iwashina, and A. Kudo, *Proc. Natl. Acad. Sci.* **109**, 11564 (2012).
- [10] A. Kudo, K. Omori, and H. Kato, *J. Am. Chem. Soc.* **121**, 11459 (1999).
- [11] R. J. Finch and J. M. Hanchar, *Rev. Mineral. Geochem.* **53**, 1 (2003).
- [12] N. Clavier, R. Podor, and N. Dacheux, *J. Eur. Ceram. Soc.* **31**, 941 (2011).
- [13] V. Panchal, D. Errandonea, F. J. Manjón, A. Muñoz, P. Rodríguez-Hernández, M. Bettinelli, S. N. Achary, and A. K. Tyagi, in *Proceedings of the 59th DAE Solid State Physics*

- Symposium 2014*, edited by D. Bhattacharyya, R. Chitra, and N. K. Sahoo, AIP Conf. Proc. 1665 (AIP, Melville, NY, 2015), p. 030006.
- [14] V. Panchal, S. López-Moreno, D. Santamaría-Pérez, D. Errandonea, F. J. Manjón, P. Rodríguez-Hernandez, A. Muñoz, S. N. Achary, and A. K. Tyagi, *Phys. Rev. B* **84**, 024111 (2011).
- [15] D. Errandonea, R. S. Kumar, S. N. Achary, and A. K. Tyagi, *Phys. Rev. B* **84**, 224121 (2011).
- [16] V. Panchal, D. Errandonea, A. Segura, P. Rodríguez-Hernandez, A. Muñoz, S. Lopez-Moreno, and M. Bettinelli, *J. Appl. Phys.* **110**, 043723 (2011).
- [17] D. Errandonea, S. N. Achary, J. Pellicer-Porres, and A. K. Tyagi, *Inorg. Chem.* **52**, 5464 (2013).
- [18] A. B. Garg, D. Errandonea, P. Rodríguez-Hernández, S. López-Moreno, A. Muñoz, and C. Popescu, *J. Phys.: Condens. Matter* **26**, 265402 (2014).
- [19] A. B. Garg, and D. Errandonea, *J. Solid State Chem.* **226**, 147 (2015).
- [20] B. Yue, F. Hong, S. Merkel, D. Tan, J. Yan, B. Chen, and H.-K. Mao, *Phys. Rev. Lett.* **117**, 135701 (2016).
- [21] G. Dreyer and E. Tillmanns, *Neues Jahrbuch für Mineralogie-5 Monatshefte* (1981), pp. 151–154.
- [22] R. S. Roth and J. L. Waring, *Am. Mineral.* **48**, 1348 (1963).
- [23] A. Sleight, H. Y. Chen, A. Ferretti, and D. Cox, *Mater. Res. Bull.* **14**, 1571 (1979).
- [24] J. W. E. Mariathasan, R. M. Hazen, and L. W. Finger, *Phase Transitions* **6**, 165 (1986).
- [25] J. Bierlein and A. Sleight, *Solid State Commun.* **16**, 69 (1975).
- [26] A. Pinczuk, B. Welber, and F. Dacol, *Solid State Commun.* **29**, 515 (1979).
- [27] R. M. Hazen and J. W. E. Mariathasan, *Science* **216**, 991 (1982).
- [28] I. G. Wood, B. Welber, W. I. F. David, and A. M. Glazer, *J. Appl. Crystallogr.* **13**, 224 (1980).
- [29] W. I. F. David, A. M. Glazer, and A. W. Hewat, *Phase Transitions* **1**, 155 (1979).
- [30] A. Pinczuk, G. Burns, and F. Dacol, *Solid State Commun.* **24**, 163 (1977).
- [31] H. Tokumoto and H. Unoki, *Phys. Rev. B* **27**, 3748 (1983).
- [32] G. Benyuan, M. Copic, and H. Z. Cummins, *Phys. Rev. B* **24**, 4098(R) (1981).
- [33] I. Tomeno, N. Sato, Y. Sato, K. Oka, and Y. Tsunoda, *Phys. Rev. B* **84**, 014302 (2011).
- [34] L. P. Avakyants, A. V. Chervyakov, V. S. Gorelik, and P. P. Sverbil', *J. Russ. Laser Res.* **25**, 535 (2004).
- [35] S. Segel, *Solid State Commun.* **54**, 403 (1985).
- [36] A. Sleight, K. Aykan, and D. Rogers, *J. Solid State Chem.* **13**, 231 (1975).
- [37] H. S. Park, K. E. Kweon, H. Ye, E. Paek, G. S. Hwang, and A. J. Bard, *J. Phys. Chem. C* **115**, 17870 (2011).
- [38] S. P. Berglund, A. J. E. Rettie, S. Hoang, and C. B. Mullins, *Phys. Chem. Chem. Phys.* **14**, 7065 (2012).
- [39] M. M. Qurashi and W. H. Barnes, *Am. Mineral.* **5**, 489 (1953).
- [40] A. J. E. Rettie, H. C. Lee, L. G. Marshall, J.-F. Lin, C. Capan, J. Lindemuth, J. S. McCloy, J. Zhou, A. J. Bard, and C. B. Mullins, *J. Am. Chem. Soc.* **135**, 11389 (2013).
- [41] A. J. E. Rettie, W. D. Chemelewski, J. Lindemuth, J. S. McCloy, L. G. Marshall, J. Zhou, D. Emin, and C. B. Mullins, *Appl. Phys. Lett.* **106**, 022106 (2015).
- [42] A. Bhattacharya, K. Mallick, and A. Hartridge, *Materials Letters* **30**, 7 (1997).
- [43] S. Klotz, J.-C. Chervin, P. Munsch, and G. L. Marchand, *J. Phys. D* **42**, 075413 (2009).
- [44] H. Mao, J. Xu, and P. Bell, *J. Geophys. Res.* **91**, 4673 (1986).
- [45] F. Datchi, R. LeToullec, and P. Loubeyre, *J. Appl. Phys.* **81**, 3333 (1997).
- [46] R. O. Jones, *Rev. Mod. Phys.* **87**, 897 (2015).
- [47] P. E. Blöchl, *Phys. Rev. B* **50**, 17953 (1994).
- [48] G. Kresse and D. Joubert, *Phys. Rev. B* **59**, 1758 (1999).
- [49] G. Kresse and J. Hafner, *Phys. Rev. B* **47**, 558 (1993).
- [50] G. Kresse and J. Hafner, *Phys. Rev. B* **49**, 14251 (1994).
- [51] G. Kresse and J. Furthmüller, *Phys. Rev. B* **54**, 11169 (1996).
- [52] G. Kresse and J. Furthmüller, *Comput. Mater. Sci.* **6**, 15 (1996).
- [53] J. Heyd, G. E. Scuseria, and M. Ernzerhof, *J. Chem. Phys.* **118**, 8207 (2003).
- [54] J. Heyd and G. E. Scuseria, *J. Chem. Phys.* **121**, 1187 (2004).
- [55] J. Paier, M. Marsman, K. Hummer, G. Kresse, I. C. Gerber, and J. G. Ángyán, *J. Chem. Phys.* **124**, 154709 (2006).
- [56] J. Heyd, G. E. Scuseria, and M. Ernzerhof, *J. Chem. Phys.* **124**, 219906 (2006).
- [57] S. López-Moreno, P. Rodríguez-Hernández, A. Muñoz, and D. Errandonea, *Inorg. Chem.* **56**, 2697 (2017).
- [58] S. López-Moreno, D. Errandonea, J. Pellicer-Porres, D. Martínez-García, S. J. Patwe, S. N. Achary, A. K. Tyagi, P. Rodríguez-Hernández, A. Muñoz, and C. Popescu, *Inorg. Chem.* **57**, 7860 (2018).
- [59] H. J. Monkhorst and J. D. Pack, *Phys. Rev. B* **13**, 5188 (1976).
- [60] K. Parlinski, Computer code phonon, <http://wolf.ifj.edu.pl/phonon>.
- [61] J. Yi, Z. Zhao, Y. Wang, D. Zhou, C. Ma, Y. Cao, and J. Qiu, *Mater. Res. Bull.* **57**, 306 (2014).
- [62] D. Errandonea and A. B. Garg, *Prog. Mater. Sci.* **97**, 123 (2018).
- [63] M. T. Dove, *Structure and Dynamics*, Oxford Master Series in Condensed Matter Physics (Oxford University Press, New York, 2003).